Supporting Information

Second-Order Nonlinear Optical Organic Crystals Based on a "Clicked" Compound

Yongshen Zheng, Junjie Guan, Puxin Cheng, Wenqing Han, Jialiang Xu* and Xian-He Bu

School of Materials Science and Engineering, Smart Sensing Interdisciplinary Science Center, Collaborative Innovation Center of Chemical Science and Engineering, Nankai University, Tongyan Road 38, Tianjin 300350, P. R. China

*E-mail: jialiang.xu@nankai.edu.cn

Experimental Section

1. Materials and Methods

All the chemicals and solvents are of reagent grade commercially purchased. Powder X-ray diffraction (PXRD) patterns were collected by a Rigaku MiniFlex600. The UV-vis absorbance spectra were obtained on a UV-vis spectrophotometer (UV 2600). Single crystal data were collected on a Rigaku XtalAB PRO MM007 DW diffractometer with Cu Kα radiation (λ = 1.5418 Å) or Mo Kα radiation (λ = 0.71073 Å). The structures were solved with the dual-direct methods using ShelxT and refined with the full-matrix least-squares technique based on F^2 using the OLEX2.[1-2] Thermogravimetric analyses (TGA) measurements were carried out under air atmosphere in a TA instruments Q50 thermal analyzer, with a constant heating rate of 10 ^{o}C/min. ^{1}H and ^{13}C NMR spectra were obtained on a Bruker 400 MHz. Mass spectrometry (MS) spectrum was obtained on a Shimadzu LCMS-2020. The thickness of samples was accessed by a Filmetrics Profilm3D profilometer. The elemental analysis was characterized by CHONS elemental analyzer (Vario EL cube). The single crystal NLO measurements were examined with a home-built scanning microscope with a femotosecond laser system (Mai Tai HP, < 100 fs, 80 MHz, spot diameter ~20 µm, wavelength tunable from 690 to 1040 nm) in the reflection geometry, with the incidence and detection angles both at 45°. The measured SHG signal is reflected from the front surface of sample and the phase-matching conditions are not considered.[3]

2. Calculations

All the DFT/TD-DFT calculations were carried out in the C.01 version of Gaussian16.[4] The B3LYP functional and 6-31G++ basis were adopted to obtain the HOMO and LUMO wavefunctions and the molecular dipole moment of BPTA S_0 state. We have selected B3LYP/6-31G+(d) basis to calculate the transition density of states from S_0 to S_1. The visualizations were displayed by VMD software.[5] The optimized structures of the individual BPTA molecule are consistent from the *α- and β-* phase, as calculated from their single crystal structures. The Hirshfeld surface calculations were implemented in CrystalExplorer.[6] The overall permanent dipole moments in a unit cell have been performed in the first-principles code Vienna ab initio simulation package (VASP).[7]

3. Synthesis

Preparation of BPTA: The synthetic route to the target compound BPTA was shown in Scheme S1. Benzyl azide (133.1 mg, 1.0 mmol), phenylacetylene (102.1 mg, 1.0 mmol), $CuSO_4$ (16.0 mg, 0.1 mmol), and sodium ascorbate (99.1 mg, 0.5 mmol) were added into the mixed solvent of methanol (3.0 mL) and water (3.0 mL). The reaction mixture was stirred at room temperature for 5 hours. Then the mixture solution was cooled and diluted with DI water. Precipitate was formed and collected by filtration. The filter cake was washed with water (3 × 25.0 mL) and then dissolved in dichloromethane. It was further purified by flash chromatography to afford the pure product. Colorless needle crystals of BPTA (216.2 mg) were obtained by recrystallization from n-heptane.

Yield ~92%. ^{1}H NMR (400 MHz, DMSO): δ 8.65 (s, 1H), 7.86 (m, 2H), 7.38 (m, 8H), 5.65 (s, 2H). ^{13}C NMR (101 MHz, DMSO): δ 147.14, 136.49, 131.15, 129.36, 129.28, 128.64, 128.36, 125.63, 122.04, 53.50. MS (ESI) m/z: $[M^{+}H]^{+}$ calcd for $C_{15}H_{13}N_3$: 235.29; found, 236.20. Anal. calcd for $C_{15}H_{13}N_3$ (%): C 76.57, H 5.53, N 17.85; found: C 76.60, H 5.72, N 17.69.

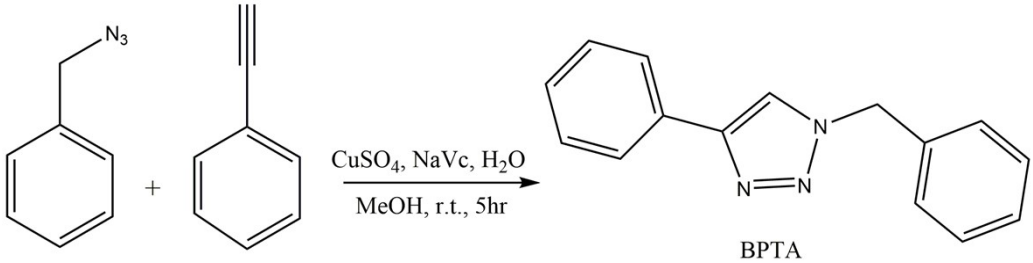

Scheme S1. Synthesis route to the target compound BPTA.

Supporting Figures

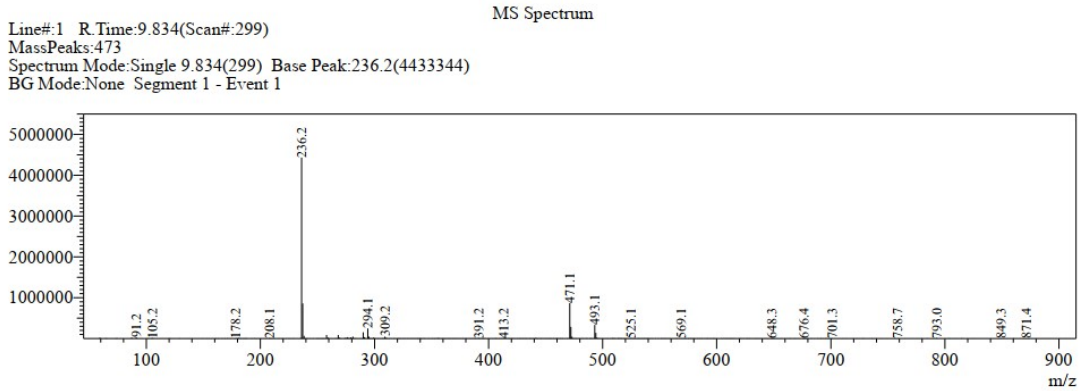

Figure S1. MS spectrum of BPTA.

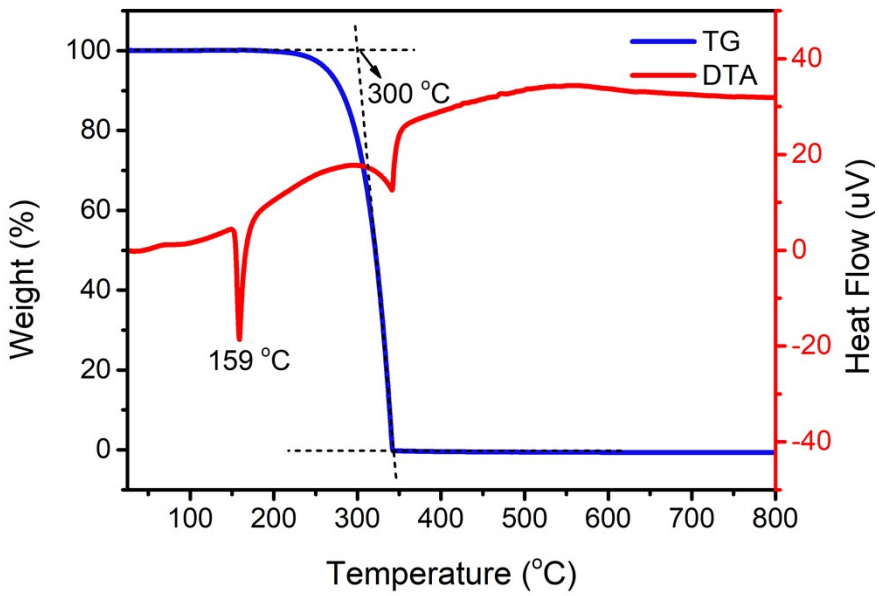

Figure S2. TGA curves of BPTA.

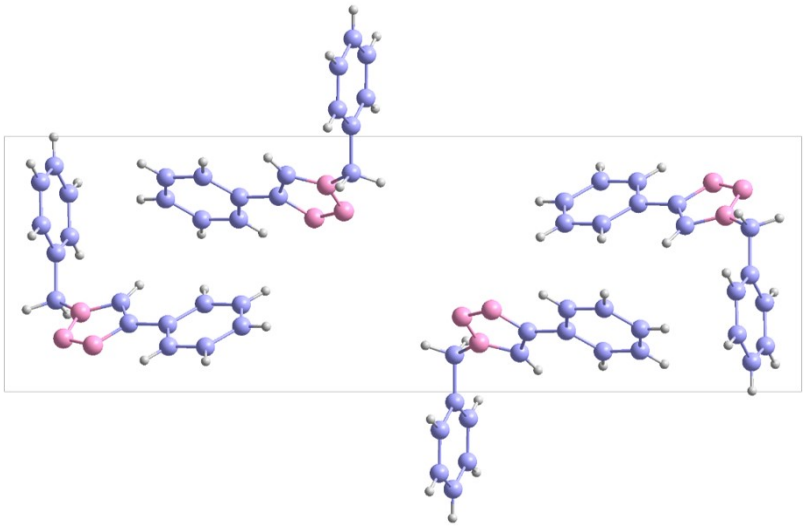

Figure S3. Molecular packing of the *γ*-phase BPTA in a unit cell viewed along the crystallographic *a*-axis.

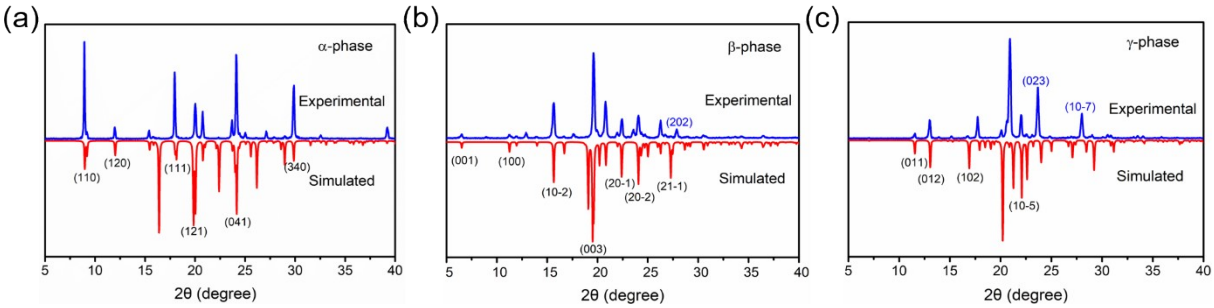

Figure S4. PXRD patterns with face indexation of the as-prepared (a) α-phase, (b) β-phase, and (c) *γ*-phase crystals, in comparison with the simulated patterns.

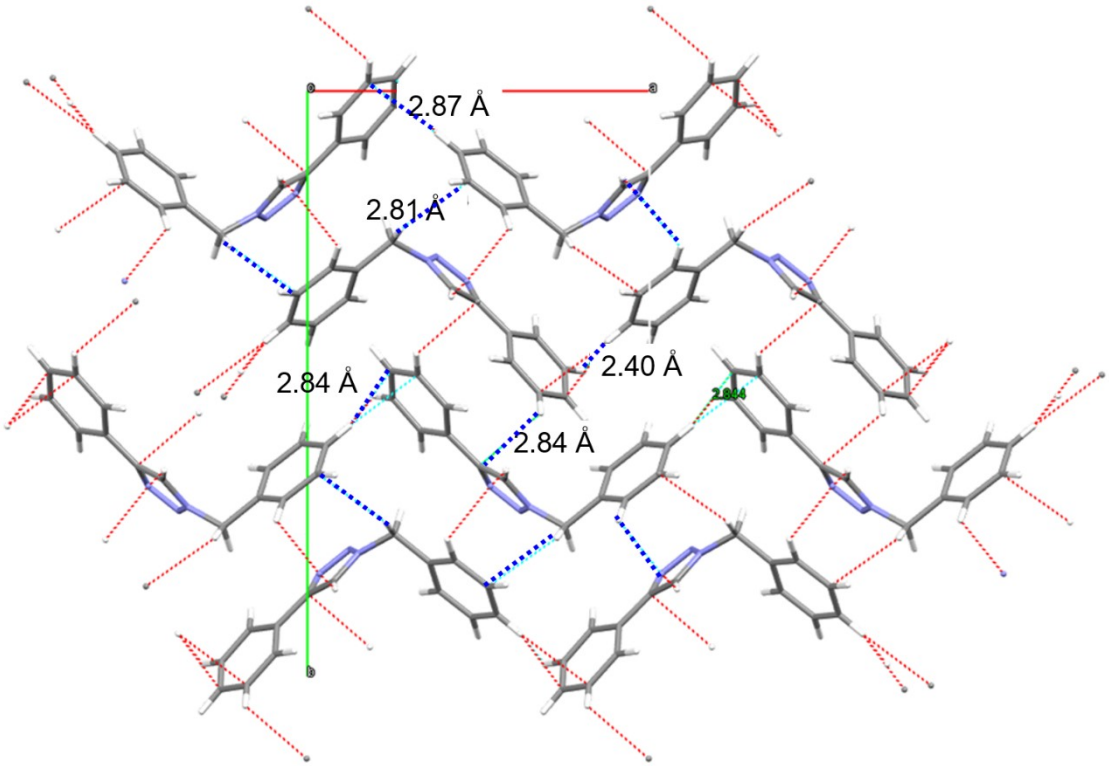

Figure S5. Intermolecular C-H…π interaction networks of the α-phase in the *aob* plane (viewed along the crystallographic *c*-axis). Dotted blue lines represent the molecular interactions. Dotted red lines represent the interaction between the shown molecule and an unshown one.

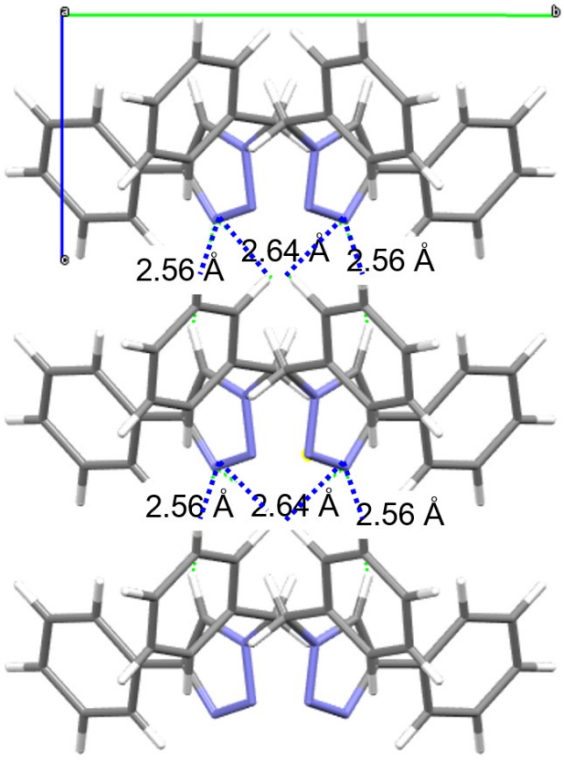

Figure S6. Intermolecular C-H…N hydrogen bonds of the α-phase viewed along the crystallographic *a*-axis.

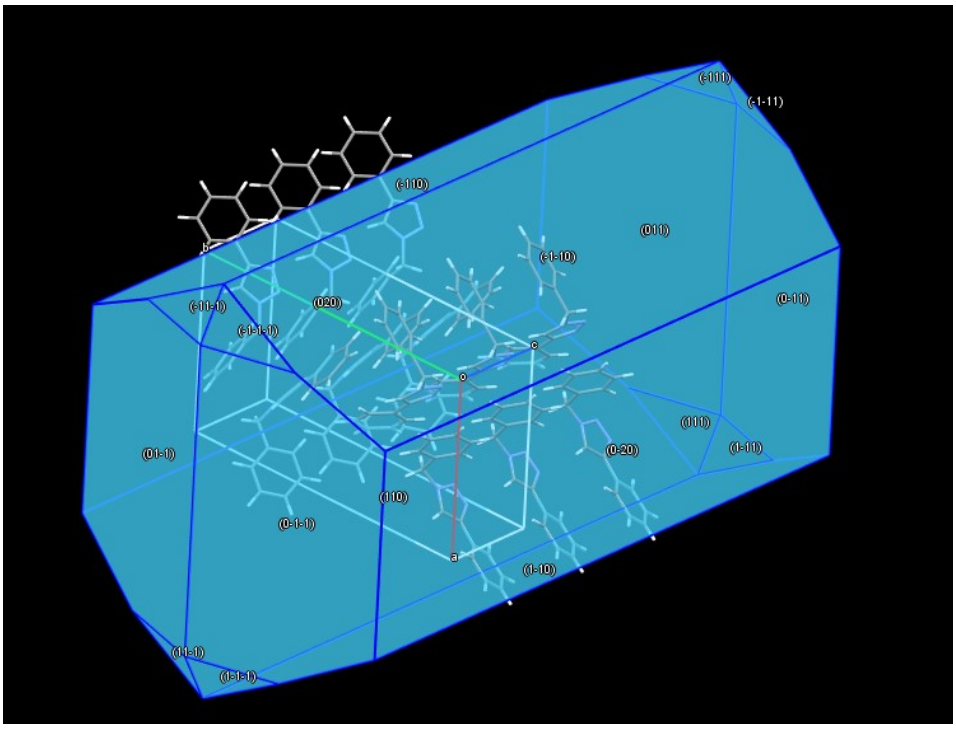

Figure S7. The calculated morphology of the α-phase with face indexation calculated by single crystal data and attachment theory.

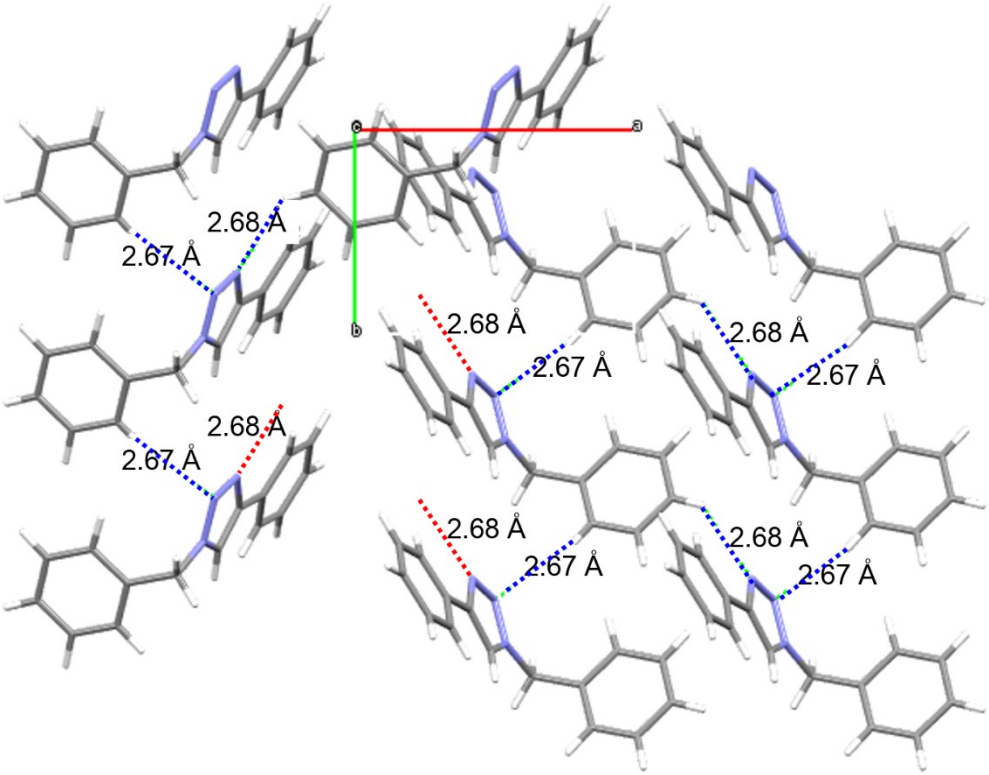

Figure S8. Intermolecular C-H…N hydrogen bonds of the β-phase in the *aob* plane (viewed along the crystallographic *c*-axis). Dotted blue lines represent the molecular interactions. Dotted red lines represent the interaction between the shown molecule and an unshown one.

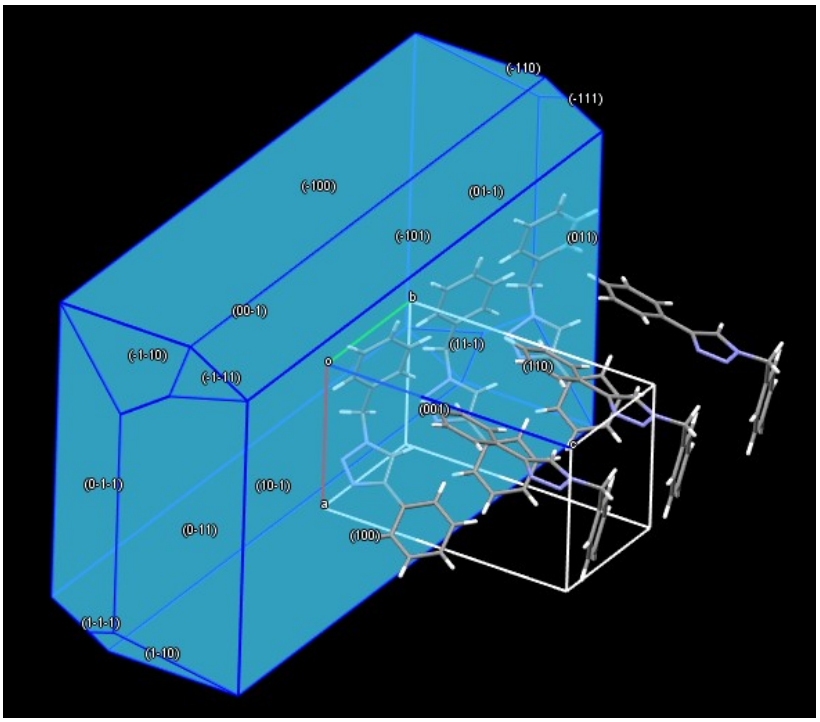

Figure S9. The calculated morphology of the β-phase with face indexation calculated by single crystal data and attachment theory.

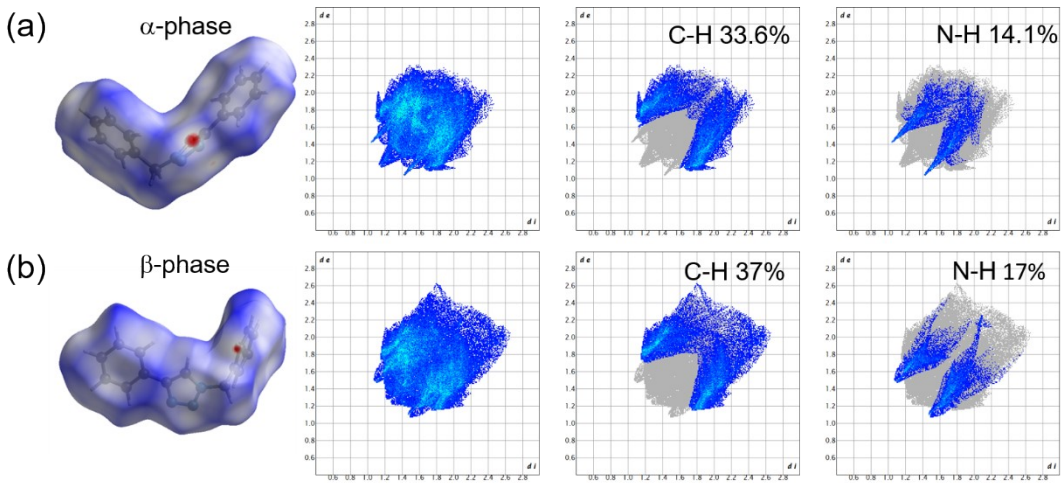

Figure S10. The Hirshfeld surfaces and the 2D fingerprint plots of BPTA in the (a) α-phase and (b) β-phase. The red area means a strong interaction, while the blue area refers to a weak one.

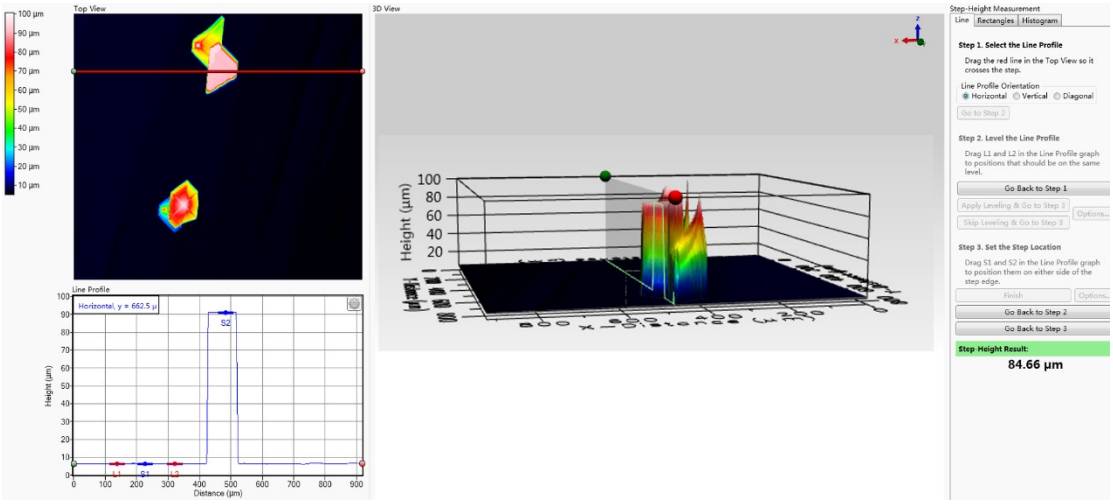

Figure S11. The thickness of the α-phase BPTA crystal (about 85 µm).

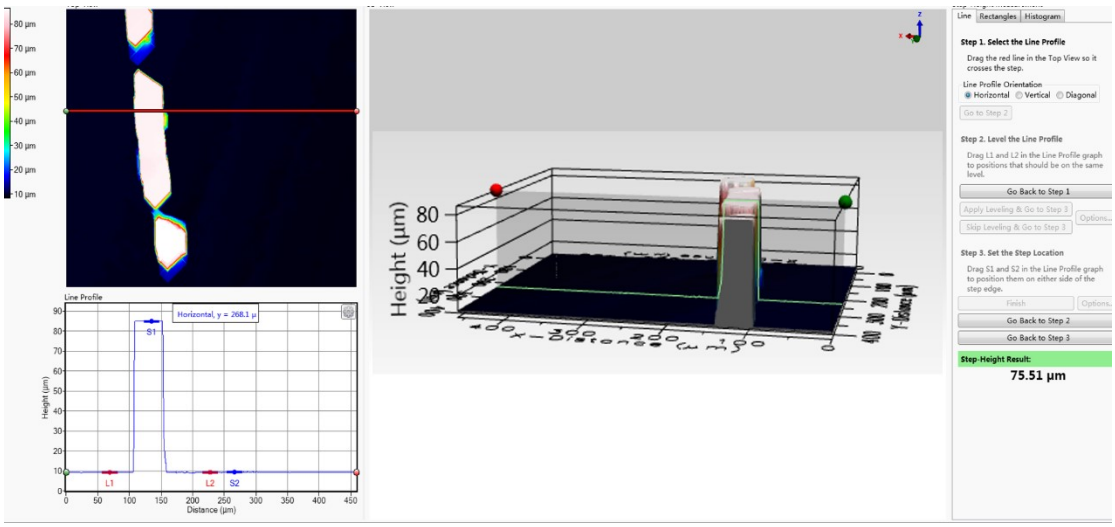

Figure S12. The thickness of the β-phase BPTA crystal (about 76 µm).

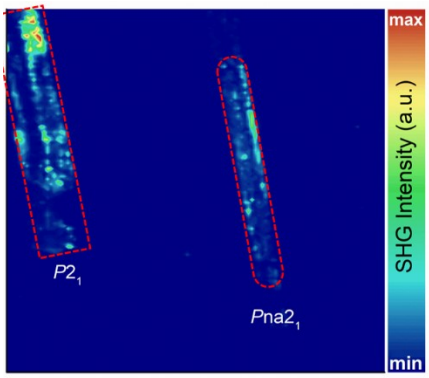

Figure S13. The SHG mapping of the α- (right) and β- phase (left) BPTA crystals. Mapping area: 1.10 × 1.40 mm^2.

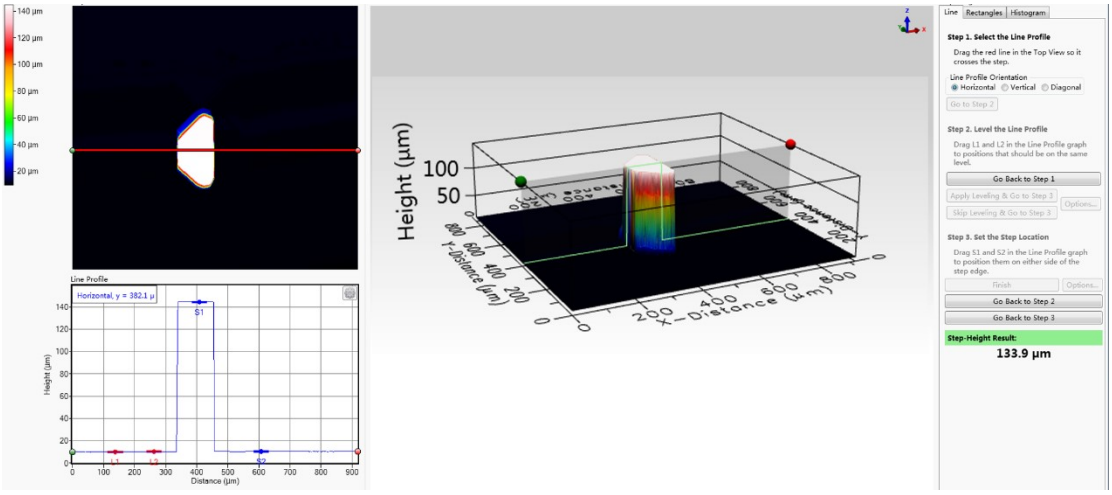

Figure S14. The thickness of KDP crystal (about 134 µm).

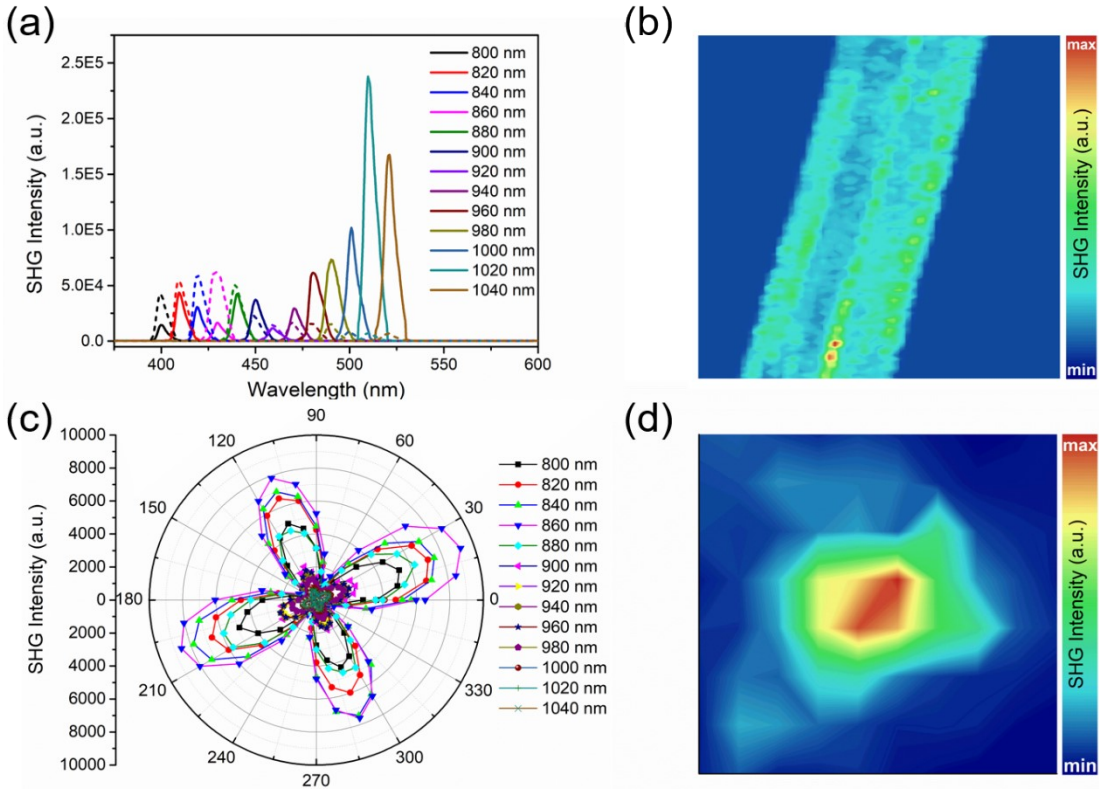

Figure S15. (a) The comparison of SHG intensity between the β-phase BPTA crystal (solid line) and the benchmark KDP crystal (dash line), at different wavelengths under the same measurement conditions. Incident power: 20 mW. (b) The SHG mapping of the β-phase BPTA crystal. Mapping area: 0.10 × 0.16 mm^2. (c) Polarization-dependent SHG spectra of KDP at different wavelengths. (d) The SHG mapping of KDP. Mapping area: 0.10 × 0.12 mm^2.

Supporting Table

Table S1. Crystal data and refinement results for BPTA.

Polymorphs	α-phase	β-phase	γ-phase
Formula	$C_{15}H_{13}N_3$	$C_{15}H_{13}N_3$	$C_{15}H_{13}N_3$
CCDC	2091945	2091943	2091944
Formula mass	235.29	235.29	235.29
Temperature (K)	100.00(10)	300.04(1)	120.00(10)
Crystal system	orthorhombic	monoclinic	monoclinic
Space group	$Pna2_1$	$P2_1$	$P2_1/c$
a (Å)	11.1253(2)	7.9806(2)	5.99714(13)
b (Å)	19.3610(3)	5.7647(10)	8.0426(2)
c (Å)	5.55420(10)	13.7805(3)	25.1397(5)
α (°)	90	90	90
β (°)	90	100.288(2)	94.4724(17)
γ (°)	90	90	90
V (Å^3)	1196.36(4)	623.79(2)	1208.86(5)
Z	4	2	4
D_c (g/cm^3)	1.306	1.253	1.293
μ (mm^{-1})	0.627	0.602	0.621
Final R indexes [I > = 2sigma (I)]	R_1 = 0.0262, wR_2 = 0.0714	R_1 = 0.0149, wR_2 = 0.0384	R_1 = 0.0239, wR_2 = 0.0663
Final R indexes [all data]	R_1 = 0.0273, wR_2 = 0.0720	R_1 = 0.0151, wR_2 = 0.0385	R_1 = 0.0255, wR_2 = 0.0673
F(000)	497.5	248.8	497.5
Index ranges	-13 ≤ h ≤ 12, -24 ≤ k ≤ 23, -6 ≤ l ≤ 3	-9 ≤ h ≤ 9, -6 ≤ k ≤ 4, -14 ≤ l ≤ 17	-7 ≤ h ≤ 6, -7 ≤ k ≤ 9, -31 ≤ l ≤ 31
GDF on F^2	1.100	1.190	1.113
Reflections collected	4419	2993	6091
Flack parameter	-0.2(3)	0.38(17)	-

Supporting References

1. O. V. Dolomanov, L. J. Bourhis, R. J. Gildea, J. A. K. Howard and H. Puschmann, OLEX2: a complete structure solution, refinement and analysis program, *J. Appl. Crystallogr.*, 2009, **42**, 339-341.
2. F. Kleemiss, O. V. Dolomanov, M. Bodensteiner, N. Peyerimhoff, L. Midgley, L. J. Bourhis, A. Genoni, L. A. Malaspina, D. Jayatilaka, J. L. Spencer, F. White, B. Grundkotter-Stock, S. Steinhauer, D. Lentz, H. Puschmann and S. Grabowsky, Accurate crystal structures and chemical properties from NoSpherA2, *Chem Sci*, 2020, **12**, 1675-1692.
3. Y. Zheng, J. Xu and X. H. Bu, 1D Chiral Lead Halide Perovskites with Superior Second-Order Optical Nonlinearity, *Adv. Optical Mater.*, 2021, **10**, 2101545.
4. Gaussian 16, Revision C.01, M. J. Frisch, G. W. Trucks, H. B. Schlegel, G. E. Scuseria, M. A. Robb, J. R. Cheeseman, G. Scalmani, V. Barone, G. A. Petersson, H. Nakatsuji, X. Li, M. Caricato, A. V. Marenich, J. Bloino, B. G. Janesko, R. Gomperts, B. Mennucci, H. P. Hratchian, J. V. Ortiz, A. F. Izmaylov, J. L. Sonnenberg, D. Williams-Young, F. Ding, F. Lipparini, F. Egidi, J. Goings, B. Peng, A. Petrone, T. Henderson, D. Ranasinghe, V. G. Zakrzewski, J. Gao, N. Rega, G. Zheng, W. Liang, M. Hada, M. Ehara, K. Toyota, R. Fukuda, J. Hasegawa, M. Ishida, T. Nakajima, Y. Honda, O. Kitao, H. Nakai, T. Vreven, K. Throssell, J. A. Montgomery, Jr., J. E. Peralta, F. Ogliaro, M. J. Bearpark, J. J. Heyd, E. N. Brothers, K. N. Kudin, V. N. Staroverov, T. A. Keith, R. Kobayashi, J. Normand, K. Raghavachari, A. P. Rendell, J. C. Burant, S. S. Iyengar, J. Tomasi, M. Cossi, J. M. Millam, M. Klene, C. Adamo, R. Cammi, J. W. Ochterski, R. L. Martin, K. Morokuma, O. Farkas, J. B. Foresman, and D. J. Fox, Gaussian, Inc., Wallingford CT, 2019.
5. W. Humphrey, A. Dalke and K. Schulten, VMD: Visual molecular dynamics, *J. Mol. Graphics*, 1996, **14**, 33-38.
6. P. R. Spackman, M. J. Turner, J. J. McKinnon, S. K. Wolff, D. J. Grimwood, D. Jayatilaka and M. A. Spackman, CrystalExplorer: a program for Hirshfeld surface analysis, visualization and quantitative analysis o molecular crystals, *J. Appl. Crystallogr.*, 2021, **54**, 1006-1011.
7. G. Kresse and J. Hafner, Ab initio molecular dynamics for liquid metals, *Phys. Rev. B*, 1993, **47**, 558-561.